Nanoscale

PAPER

View Article Online
View Journal | View Issue

Cite this: *Nanoscale*, 2015, **7**, 7644

High pressure pyrolyzed non-precious metal oxygen reduction catalysts for alkaline polymer electrolyte membrane fuel cells†

Jakkid Sanetuntikul and Sangaraju Shanmugam*

Received 15th January 2015,
Accepted 18th March 2015

DOI: 10.1039/c5nr00311c

www.rsc.org/nanoscale

Non-precious metal catalysts, such as metal-coordinated to nitrogen doped-carbon, have shown reasonable oxygen reduction reaction (ORR) performances in alkaline fuel cells. In this report, we present the development of a highly active, stable and low-cost non-precious metal ORR catalyst by direct synthesis under autogenic-pressure conditions. Transmission electron microscopy studies show highly porous Fe–N–C and Co–N–C structures, which were further confirmed by Brunauer–Emmett–Teller surface area measurements. The surface areas of the Fe–N–C and Co–N–C catalysts were found to be 377.5 and 369.3 $m^2\ g^{-1}$, respectively. XPS results show the possible existence of N–C and M–N_x structures, which are generally proposed to be the active sites in non-precious metal catalysts. The Fe–N–C electrocatalyst exhibits an ORR half-wave potential 20 mV higher than the reference Pt/C catalyst. The cycling durability test for Fe–N–C over 5000 cycles shows that the half-wave potential lost only 4 mV, whereas the half-wave potential of the Pt/C catalyst lost about 50 mV. The Fe–N–C catalyst exhibited an improved activity and stability compared to the reference Pt/C catalyst and it possesses a direct 4-electron transfer pathway for the ORR process. Further, the Fe–N–C catalyst produces extremely low HO_2^- content, as confirmed by the rotating ring-disk electrode measurements. In the alkaline fuel single cell tests, maximum power densities of 75 and 80 mW cm^{-2} were observed for the Fe–N–C and Pt/C cathodes, respectively. Durability studies (100 h) showed that decay of the fuel cell current was more prominent for the Pt/C cathode catalyst compared to the Fe–N–C cathode catalyst. Therefore, the Fe–N–C catalyst appears to be a promising new class of non-precious metal catalysts prepared by an autogenic synthetic method.

Introduction

Electrochemical oxygen reduction is a key reaction for energy conversion technologies.[1–4] Recently, great attention has been given to using non-precious metal catalysts for oxygen reduction reactions (ORRs) in polymer electrolyte fuel cells to replace the Pt-based catalysts and reduce the cost of fuel cell technology. Therefore, significant research has been focused on the development of non-precious metal catalysts owing to their high activity, stability, and possible use over a wide range of pH values.[5–7]

Research on non-precious metal catalysts has been continually pursued since the key research initiated by Jasinski,[8] who used metal phthalocyanine based catalysts for the ORR in an alkaline medium. In later studies, the development of highly active and durable non-precious metal catalysts based on heteroatom doped-carbon[9–12] or metal coordinated with nitrogen-doped carbon (M–N–C, M = Fe, Co or FeCo), synthesized by the heat-treatment of various precursors from 700 to 1000 °C under an inert gas atmosphere, resulted in ORR catalysts with superior activity and stability.[9–11,13] An excellent example of a non-precious metal catalyst has been described by Chung *et al.*[14] using iron acetate as the metal source, cyanamide as the nitrogen source and functionalized black pearls (carbon 2000) as the carbon source, and then direct pyrolysis at a high temperature under a N_2 atmosphere. This catalyst exhibits better stability and activity compared with Pt/C with a high loading of 1 mg cm^{-2} and the presence of Fe–N_4 active sites are responsible for the significant improvement in the ORR activity. Wu *et al.*[15] reported a highly active ORR catalyst, which showed comparable activity to that of commercial Pt/C and exhibited a superior durability up to 700 h at 0.4 V. This catalyst was synthesized using Fe(III) chloride, polyaniline (PANI) and Ketjenblack. The solid mixture was heat-treated under a N_2 atmosphere at 900 °C, then acid-treated in 0.5 M H_2SO_4 at 80 °C for 8 hours to remove any unstable phases, and

Department of Energy Systems Engineering, Daegu Gyeongbuk Institute of Science and Technology (DGIST), Daegu, 711-873, Republic of Korea.
E-mail: sangarajus@dgist.ac.kr; Fax: (+82) 53-785-6409

† Electronic supplementary information (ESI) available: Experimental details, additional TEM images, additional results. See DOI: 10.1039/c5nr00311c

then the precipitate catalyst underwent a second heat treatment under N_2 as the final step of the synthesis. Tan *et al.*[16] fabricated a MnO–mesoporous-N–C composite by first mixing precursors $Mn(NO_3)_2$, aniline and $KMnO_4$ in an autoclave, then the solid precipitate was collected and then pyrolysed under an Ar atmosphere at 900 °C for 4 h. The resultant product was treated with acid, washed and dried before further characterization. They found that the half-wave potential of the MnO–mesoporous-N–C catalyst was 50 mV lower than the Pt/C catalyst. Proietti *et al.*[17] created an excellent M–N–C catalyst by mixing ferrous acetate, phenanthroline and a metal–organic framework (MOF), followed by direct pyrolysis, first under an Ar atmosphere and then under an ammonia atmosphere, to obtain the electrocatalyst. The highly porous cathode catalyst showed a power density of 0.75 W cm^{-2} at 0.6 V in a H_2–O_2 single cell system, which is comparable with a commercial Pt-based catalyst, and excellent stability even in a H_2–air system. According to the aforementioned examples, non-precious metal carbon based catalysts obtained *via* the pyrolysis of precursors containing metal, nitrogen and carbon have been demonstrated to be active ORR catalysts. However, the pyrolysis of the precursor is usually carried out at a high temperature under an inert gas atmosphere, which prevents the complete decomposition of the carbon mass, leading to a poor ORR carbon based catalyst.

We initiated a research project to develop an excellent M–N–C electrocatalyst with high porosity to improve the active-site density, O_2 transport and ion-conductivity using a highly autogenic-pressure method at high temperature without using any inert gas atmosphere. The ORR activity of the M–N–C catalyst was quantified from rotating disk electrode (RDE) and rotating ring disk electrode (RRDE) measurements, and the obtained results were correlated with the active sites of N–C and M–N_x to provide the electrode material characteristics that are responsible for the high ORR activity. Further, we constructed a membrane electrode assembly using M–N–C as the cathode catalyst and an alkaline membrane, and the results are presented. In this report, we propose the synthesis of Fe–N–C and Co–N–C catalysts by an autogenic-pressure method. N_2, NH_3 or Ar atmospheres were not used during the pyrolysis in the first heat-treatment or second heat-treatment. The Fe–N–C and Co–N–C catalysts prepared by this method show superior activity and stability in an alkaline environment.

Experimental

Preparation of the electrocatalysts

The M–N–C electrocatalysts were prepared by facile direct pyrolysis under autogenic-pressure conditions. First, we synthesized a precursor by mixing melamine (3.5 g), iron acetate or cobalt acetate (1.0 g), and oxidized carbon powder (1.0 g) (VXC-72R in 60% nitric acid at 90 °C for 6 h) in ethanol at 60 °C overnight. Then, the solvent was evaporated at 45 °C and the remaining powder was converted to the electrocatalyst using direct pyrolysis under autogenic-pressure with a Swagelok union closed cell at 900 °C for 1 h with a heating rate of 10 °C min^{-1}. One hundred milligrams of the as-synthesized precursor was acid treated in 5 mL of 0.5 M H_2SO_4 at 90 °C for 6 h to remove unreacted metallic compounds and then washed with copious amounts of water until the pH was neutral. The product was then dried overnight in a vacuum oven. For the final step, the acid treated catalyst was heat-treated for a second time using a Swagelok closed cell at 900 °C for 1 h, which resulted in the Fe–N–C and Co–N–C catalysts.

Physical characterization of the catalysts

The morphologies of the catalysts were analyzed by a field-emission scanning electron microscope (FE-SEM, Hitachi, S-4800II) with an acceleration voltage of 3 kV. Before the SEM observations, the samples were coated with osmium in a vacuum chamber. The microstructures of the samples were determined by a field-emission transmission electron microscope (FE-TEM, Hitachi, HF-3300) with an acceleration voltage of 300 kV. For the TEM analysis, the samples were ultrasonically dispersed in isopropyl alcohol, and then a drop of the dispersion was deposited on a copper grid and dried under an UV lamp. The crystal structures of the samples were investigated by powder X-ray diffraction (XRD, PANalytical-Empyrean) using Cu Kα radiation, a generator voltage of 40 kV and a tube current of 30 mA. Raman spectra were obtained by using a Thermo Nicolet ALMEGA XR (Thermo Scientific) with 514 nm excitation lasers and the sample powders were prepared on a glass surface with the laser focused through a 100X microscope for a total interrogation spot size of 1 micron. The crystal structure and elemental analysis studies were performed by using an X-ray photoelectron spectroscope (XPS, Thermo Fisher Scientific, ESCALAB250 XPS system, Theta Probe XPS system) with monochromated Al K-alpha source at 15 kV and 150 W. Binding energy values on the *X*-axis were calibrated using C1s from a carbon value taken as 284.6 eV.

Electrochemical characterization of the catalysts

The ORR activities of the electrocatalysts were carried out using rotating disk electrode (RDE) and rotating ring-disk electrode (RRDE) techniques using Biologic, VSP. A three electrode system was used consisting of glassy carbon, Pt wire and a saturated calomel electrode (SCE), which acted as the working electrode, counter electrode and reference electrode, respectively. All potentials were converted to the RHE scale by adding 0.991 V, according to literature experiments.[18,19] The catalyst ink for the electrochemical measurements was prepared by dispersing 5 mg of the catalyst in 250 μL of DI-water, 20 μL of Nafion (5%), and 500 μL of isopropyl alcohol, and then ultrasonicating for 30 min to obtain a homogenous ink. From this, the catalyst ink was loaded on a clean glassy carbon electrode with 0.6 mg cm^{-2} and 0.4 mg cm^{-2} for the RDE and RRDE experiments, respectively. The catalyst loading for the reference Pt/C electrode was 30 μg cm^{-2} in both cases. The ORR experiments were carried out in O_2-saturated 0.1 M KOH electrolyte at a scan rate of 10 mV s^{-1} at ambient temperature. A flow of O_2 was maintained over the electrolyte during the

measurements to ensure the O_2 atmosphere inside the cell remained constant. For comparison, a commercial reference Pt/C electrode (10 wt%, Johnson Matthey) was used for the half-cell studies.

Fuel cell testing

The alkaline fuel cell was evaluated by making membrane electrode assemblies (MEAs). The commercial alkaline exchange membrane (Tokuyama, A201) was used to make the MEA. The membrane was treated by dipping it in 1 M KOH for 24 h, then washed with DI-water until the pH was neutral. The catalyst ink was prepared by dispersing the catalyst powder in DI-water and 40 wt% ionomer solution (Tokuyama, AS-4 ionomer) followed by isopropyl alcohol. The resultant homogeneous ink was accomplished by ultrasonicating the contents for 30 min. The catalyst layers, 40 wt% Pt/C catalyst (Johnson Matthey) and the Fe–N–C catalyst, were used as the anode and cathode, respectively. The catalyst was brushed onto diffusion-layer coated carbon papers (SGL, thickness = 0.27 mm) to make the diffusion-electrode. The anode catalyst loading was 0.5 mg_{Pt} cm^{-2}. The cathode catalyst, Fe–N–C, loading was 4 mg cm^{-2}. For comparison, a reference cathode catalyst of 40 wt% Pt/C was prepared in a similar manner to the anode. A single cell MEA was obtained by compressing the membrane between the cathode and anode at 80 °C and 15 kg cm^{-2} for 2 min. Fuel cell performance tests were carried out at 60 °C using humidified H_2–O_2 (100% relative humidity (RH), flow rate, 0.4 L min^{-1}). Before conducting the polarization plots, the MEAs were left under open-circuit voltage conditions for 3 h with 100% RH until the system reached steady state point. All the MEAs were evaluated in single cells under atmospheric pressure without applying any back pressure.

Results and discussion

Fig. 1a and b show the SEM images of the Fe–N–C and Co–N–C catalysts. They reveal high porosities, uniform particle size distributions and no agglomeration. The diameter of the particles is about 30 nm, which corresponds to the size of the VXC-72R carbon structure, as further evidenced by the TEM images (Fig. 1c and d). Furthermore, the TEM images reveal some small metal particles encapsulated in the porous carbon.

X-ray diffraction (XRD) studies were carried out for the acid treated Fe–N–C and Co–N–C catalysts to determine the crystalline structures (Fig. 2a). The XRD patterns of the two catalysts show broad graphitic C(002) and C(100) peaks, indicating a typical turbostratic carbon structure.[20] The C(002) planes of the Fe–N–C and Co–N–C catalysts were found to be at 24.5° and 24.9°, respectively. The shift to the lower angle (2θ) for the C(002) plane suggests an increase in the interlayer-distance that is related to N-doping in the carbon structure, and potentially further doping of the Fe atom as well.[21] To evaluate the nature of the carbon structure, Raman spectra were acquired for the Fe–N–C and Co–N–C catalysts. The Raman spectra show characteristic carbon peaks at ~1360 cm^{-1} (D-band) and

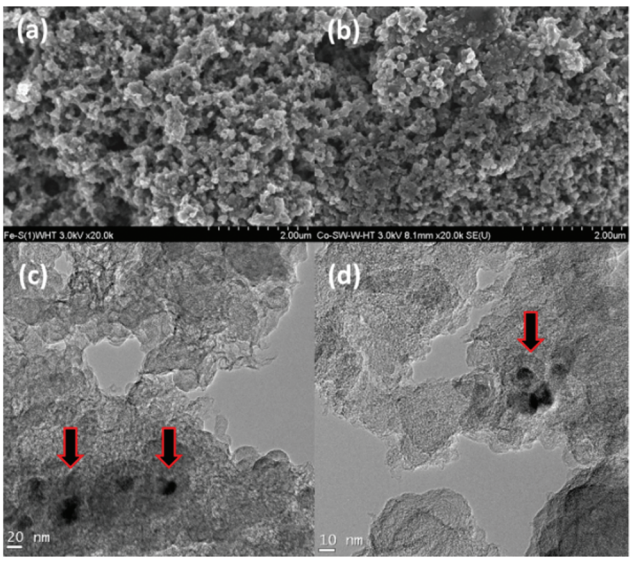

Fig. 1 Typical SEM micrographs of the (a) Fe–N–C and (b) Co–N–C catalysts. HRTEM images of the (c) Fe–N–C and (d) Co–N–C catalysts, where the arrows in each image designate the catalyst containing metal nanoparticles.

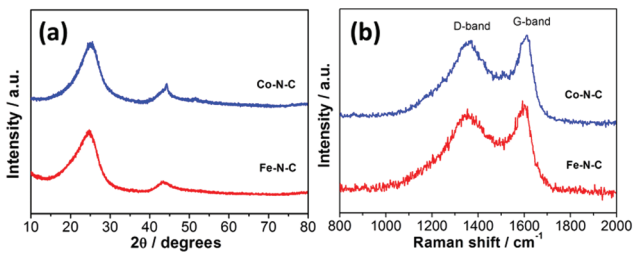

Fig. 2 (a) XRD patterns, and (b) Raman spectra of the Fe–N–C and Co–N–C catalysts.

~1590 cm^{-1} (G-band), as shown in Fig. 2b. The D-band corresponds to sp^3 defect sites, while the G-band relates to the sp^2-hybridized carbon layer.[22] The ratios of the I_D and I_G bands (I_D/I_G) were used to identify the overall quality of the carbon present in the catalysts. The values of the I_D/I_G ratios for the Fe–N–C and Co–N–C catalysts were 0.91 and 0.89, respectively. Surface area of the catalyst is very important for electrochemical ORRs. The Brunauer–Emmett–Teller (BET) surface areas of the Fe–N–C and Co–N–C samples were found to be 377.5 and 369.3 m^2 g^{-1}, respectively. According to the IUPAC guidelines, a material with an average pore size between 2 and 50 nm is termed as a mesoporous material. The pore size distributions of the Fe–N–C and Co–N–C catalysts showed average pore sizes of 3.61 and 3.63 nm, respectively. This result indicates the presence of mesopores in the M–N–C catalysts.

The XPS survey spectra of the Fe–N–C and Co–N–C catalysts revealed the presence of Fe, Co, C, O, and N (Fig. S5, ESI†). The spectrum in Fig. 3a shows a broad Fe2$p_{3/2}$ peak, which can be deconvoluted into two peaks with binding energy

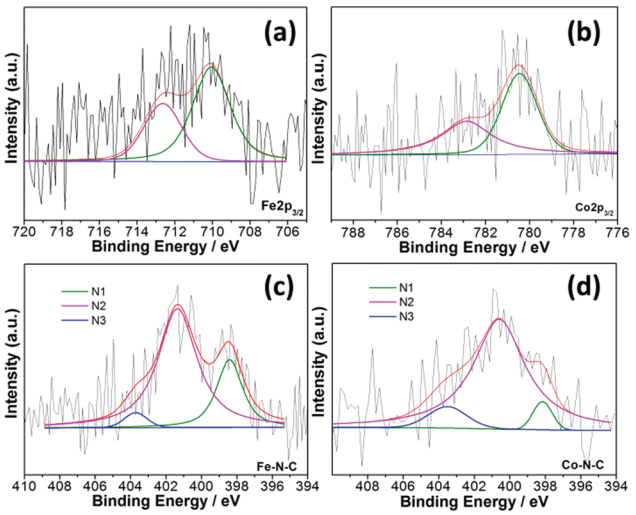

Fig. 3 High resolution XPS for (a) $Fe2p_{3/2}$ (b) $Co2p_{3/2}$ and N1s spectra of the (c) Fe–N–C, and (d) Co–N–C catalysts.

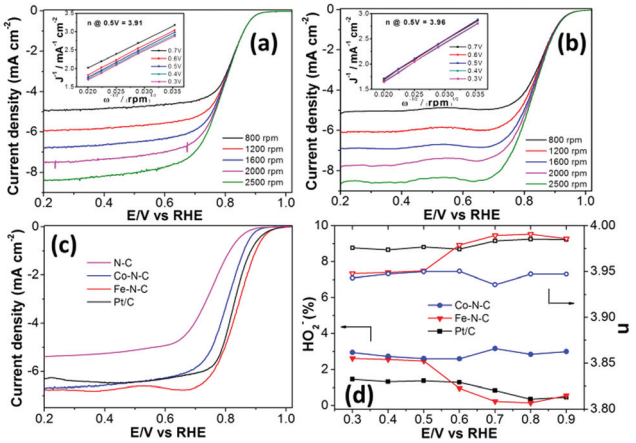

Fig. 4 Polarization curves of the (a) Co–N–C and (b) Fe–N–C catalysts in an O_2-saturated 0.1 M KOH solution at different rotation speeds (insets in (a) and (b) are the Koutecky–Levich plots of the Co–N–C and Fe–N–C catalysts, respectively). (c) Linear sweep voltammogram (LSV) curves for the Co–N–C, Fe–N–C, and Pt/C catalysts in an O_2-saturated 0.1 M KOH solution at 1600 rpm, and (d) electron transfer number and percentage of peroxide formation for the catalysts at different potentials obtained from the RRDE experiments.

values of 712.8 and 710.1 eV. These can be assigned to the Fe(II) ion[21] and Fe(III) ion,[23] respectively. Fig. 3b shows a $Co2p_{3/2}$ broad peak, which can be fitted into two peaks with binding energy values of 780.3 and 782.3 eV. These can be assigned to Co(II)O[24] and Co–N_x,[24,25] respectively. The XPS data confirmed that no zero valent metals are observed, and that the metal exists as M(II), which bonds to the N forming M–N_x species. The corresponding fitting results are given in Table S1, ESI.† The total nitrogen content measured by XPS for the Fe–N–C and Co–N–C catalysts was found to be 3.08 and 1.31 at%, respectively. High resolution N1s spectra was deconvoluted into three peaks with binding energy values of 398.3, 400.9, and 403.2 eV for the Fe–N–C and Co–N–C catalysts, which can be assigned to pyridinic-type,[19,26] pyrolic-type[27] and graphitic-type[28] nitrogen functional groups, respectively. In fact, the peak at 398.3 eV may also include the presence of the N-bond with the metal. The pyridinic nitrogen (398.0–398.5 eV) bond and N–metal (398.6–398.9 eV) are very difficult to distinguish, so the Fe–N–C catalyst showed a higher pyridinic-type nitrogen (35.7%) content than the Co–N–C catalyst (24.4%). As discussed above, this correlates well with the ORR results, which will be discussed in a later section. Furthermore, the quantitative analyses of the M–N–C samples revealed the ratio of N to C (N/C ratio) of the Fe–N–C and Co–N–C catalysts to be 0.033% and 0.014%, respectively. The N/C ratios observed using XPS were in good agreement with the results observed by elemental analysis (Tables S1 and S2, ESI†).

To evaluate the ORR performance of the Fe–N–C and Co–N–C catalysts, a rotating-disk electrode (RDE) was used in an O_2-saturated 0.1 M KOH solution at a scan rate 10 mV s^{-1} (Fig. 4a and b). The ORR polarization curves recorded from 800 to 2500 rpm show that the current increased as the rotating speed was increased, which can be explained by the shortening flux-diffusion resulting in increasing currents. The results were compared with a commercial Pt/C catalyst (10% Pt/C, Johnson Matthey). Fig. 4c shows the comparison between the ORR properties of the non-precious metal catalysts with those of the Pt/C catalyst in 0.1 M KOH at 1600 rpm. The ORR onset potential of the Fe–N–C catalyst is nearly the same as that of the reference Pt/C catalyst with a loading of 30 μg_{Pt} cm^{-2} (1.05 V *vs.* RHE) and higher than that of the Co–N–C catalyst. More importantly, the half-wave potentials ($E_{1/2}$) of the Fe–N–C and Co–N–C catalysts were 0.86 and 0.81 V *vs.* RHE, respectively, while the Pt/C catalyst shows an $E_{1/2}$ value of 0.84 V. The $E_{1/2}$ value of the Fe–N–C catalyst is 20 mV higher than that of the Pt/C catalyst and 50 mV higher than that of the Co–N–C catalyst. The addition of transition metal elements leads to activity enhancement of the catalysts relative to the nitrogen-doped functionalized VXC-72R carbon (N–C) catalyst, as shown in Fig. 4c. The Koutecky–Levich (K–L) plots shown as insets in Fig. 4a and b are derived from the polarization curves and these plots show good linearity and parallelism over all the potential range, suggesting first order reaction kinetics for the oxygen reduction reaction. The electron transfer numbers (n) are 3.96 and 3.91 for the Fe–N–C and Co–N–C catalysts, respectively, at 0.5 V *vs.* RHE, suggesting that both catalysts exhibited a direct four-electron process.[29] From these results, the enhanced ORR activity of the Fe–N–C catalyst is attributed to: (i) the total doped-nitrogen content in the carbon network (N/C ratio) of the Fe–N–C catalyst is higher than for the Co–N–C catayst, (ii) the Fe–N–C catalyst exhibits a higher pyridinic-type nitrogen content, which are considered to be ORR active sites and, (iii) based on the XPS data, the Fe and Co contents in the M–N–C catalysts are quite similar. However, the Fe–N–C catalyst exhibited a higher N-content. Therefore, the probability of creating M–N_x moieties or N–C in the Fe–N–C catalyst is higher than in the Co–N–C catalyst.

Adding a metal precursor during the synthesis showed an enhancement in the ORR performance compared to N-doped carbon. The introduction of M atoms is more likely to create $M–N_4$ moieties in the catalyst. Generally, metal-ion centers are considered to be more active for ORRs, which could be correlated to the increased binding capabilities of oxygen and higher ionization potentials. We can conclude that Fe–N–C is a highly active catalyst. This indicates that the synthesis of electrocatalysts under autogenic-pressure appears to be a promising method to synthesize the Fe–N–C catalyst and the activity of such a catalyst is comparable with other ORR catalysts based on carbon nanotubes (CNTs),[14] porous structures[29] or graphene.[30] In fact, we also tested the ORR activity of the Fe–N–C catalyst under acidic electrolyte conditions, which showed a good diffusion-limited current and the $E_{1/2}$ potential was only 50 mV lower than the reference Pt/C catalyst (Fig. S6, ESI†).

The formation of peroxide species (HO_2^-) during the ORR process was analyzed by a rotating-ring disk electrode (RRDE). The ring and disk currents recorded at 1600 rpm in an O_2-saturated 0.1 M KOH solution for the Fe–N–C and Co–N–C catalysts were compared with reference Pt/C catalyst (Fig. S7, ESI†). The percentage of HO_2^- and the number of electrons transferred (n) derived from the RRDE experiments (Fig. 4d) are the same values of ~3% and ~3.95, respectively, over the potential range of 0.3–0.9 V, which are in good agreement with the electron transfer number observed from the RDE experiments. Interestingly, the Fe–N–C and Co–N–C catalysts exhibit extremely low HO_2^- percentages and a higher number of electron transferred under alkaline conditions. For the ORR process with a non-precious metal catalyst, an oxygen molecule can reduce to HO_2^- at a M–N–C or N–C active site and further reduce again at a metal-oxide site, as suggested by Mukerjee *et al.*,[31] and a bi-functional mechanism can be observed. The ORR process mainly occurs at $Fe–N_x$ and $Co–N_x$, and then the intermediate HO_2^- can also be captured by the metal-oxide particle, which is encapsulated directly in the carbon pores (see TEM images in Fig. 1 and Fig. S2, ESI†). A similar report has been published by Liang *et al.*,[32] where the interaction of N-graphene and Co_3O_4 on Co_3O_4/N-graphene catalyst composites can improve the ORR performance. We believe that the high synergy of $M–N_x$ and a small amount of metal-oxide greatly contributes to the enhanced ORR performance.

The cycling durability test of the Fe–N–C catalyst was carried out and compared with a Pt/C catalyst by performing repeated potentiodynamic cycling for 5000 cycles over a potential range of 0.6–1.0 V *vs.* RHE at a scan rate of 50 mV s^{-1} (Fig. 5). After 5000 cycles, the $E_{1/2}$ value of the Fe–N–C catalyst showed a small loss of about 4 mV, while the Pt/C catalyst showed a 50 mV negative shift. These results indicate that the surface properties of the non-precious metal catalyst were maintained during the potential cycling test. The degradation of the Pt/C and Fe–N–C catalysts are different because Pt particles suffer from Pt agglomeration, Pt dissolution and degradation of the carbon support at high potential that lead to degradation of the Pt/C catalyst. However, the Fe–N–C catalyst can degrade in terms of the carbon material and oxidation of the active sites.[33]

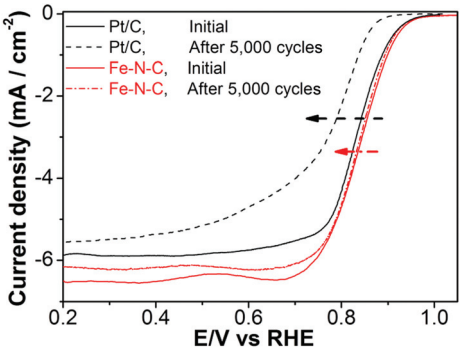

Fig. 5 Polarization curves of the Fe–N–C and Pt/C catalysts during the cycling durability tests in an O_2-saturated 0.1 M KOH solution at 1600 rpm (cycling tests were carried out over a potential range of 0.6–1.0 V *vs.* RHE with 50 mV s^{-1}).

MEA fuel cell tests of a catalyst are important for practical applications. The comparison of alkaline membrane fuel cells with Fe–N–C (loading: 4 mg cm^{-2}) and commercial Pt/C (40% Pt/C-JM, loading: 0.5 mg_{Pt} cm^{-2}) as the cathode catalysts for a single cell $H_2–O_2$ gas system at 60 °C is shown in Fig. 6. The open circuit voltage (OCV) values of Fe–N–C, Co–N–C and Pt/C were 1.04, 0.99 and 1.04 V, respectively. The maximum power densities (P_{max}) of Fe–N–C, Co–N–C and Pt/C were 75, 68 and 80 mW cm^{-2}, respectively. The alkaline fuel cell performance of the Fe–N–C electrode was almost comparable to that of the Pt/C electrode. Further, the Fe–N–C catalyst displayed behaviour like the Pt/C catalyst over all the current density region, demonstrating that the Fe–N–C electrocatalyst was highly active in the ORR process. The value of P_{max} compares to other non-precious metal cathode catalysts, as summarized and listed in Table S3, ESI.† The performances of Fe–N–C and Pt/C as cathode catalysts are low compared with the work by Kruusenberg *et al.*[34] The cathode catalyst, type of alkaline membrane, the fuel cell operating conditions (temperature, humidity, pressure, flow rate of gas, back pressure, water-

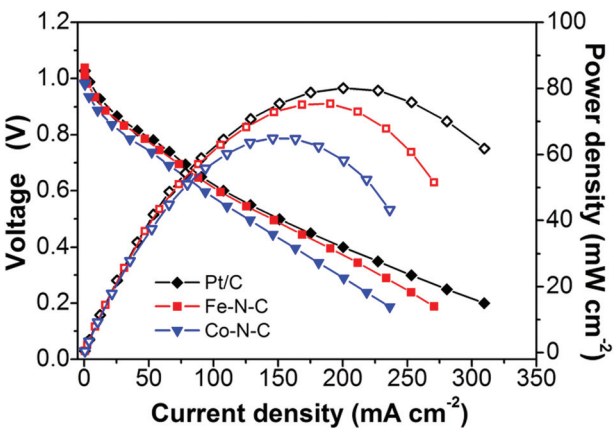

Fig. 6 Alkaline membrane fuel cell performance of MEA with Fe–N–C and Pt/C as the cathode at 60 °C.

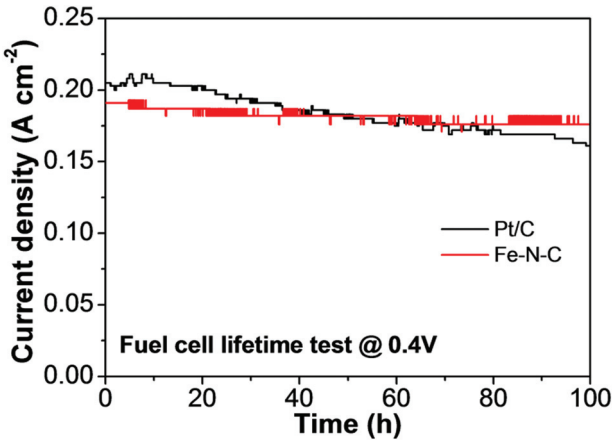

Fig. 7 Alkaline membrane fuel cell performance durability tests at a constant voltage of 0.4 V in H_2–O_2 for a MEA with Fe–N–C and Pt/C as cathode based catalysts at 60 °C.

transport in the electrode) and MEA fabrication techniques have to be considered for optimization. Further studies are underway using different alkaline exchange membranes and MEA fabrication techniques to measure the power density of M–N–C catalysts.

The fuel cell 100 hours durability tests under 100% RH at 60 °C, with a constant voltage of 0.4 V for the Fe–N–C catalyst and the reference Pt/C catalyst are shown in Fig. 7. The fuel cell durability test of the Pt/C cathode catalyst shows that the current decay is faster than for the Fe–N–C catalyst. The best durability was obtained with the Fe–N–C catalyst, with a drop in current density of only 8% at 0.4 V, while the Pt/C catalyst showed a loss of ~20%. The high durability of the Fe–N–C electrode indicates a promising electrocatalyst for oxygen reduction in alkaline membrane fuel cells. Advanced surface characterization studies are needed to clarify the M–N–C activity, and the durability of the catalyst is also an important feature that must be tested for more hundreds/thousands of hours within a fuel cell to be considered for applications.

Conclusions

In summary, we present a highly active non-precious metal ORR catalyst that was prepared by a simple method using direct pyrolysis without purging any gases in a specially made cell. In the synthesis, the nitrogen and metal source, including carbon, play important roles to make porous M–N–C electrode materials with ORR active sites. The ORR results reveal that the Fe–N–C catalyst with a loading of 0.6 mg cm^{-2} showed an $E_{1/2}$ potential higher than the reference Pt/C catalyst with 30 μg cm^{-2} catalyst loading. Furthermore, the Fe–N–C catalyst provides a direct 4-electron pathway and superior durability towards ORRs in alkaline medium. In the single cell test, the Fe–N–C cathode catalyst provides a maximum power density comparable to commercial Pt/C and a better long-term stability for 100 h, which indicates good activity for the catalyst. The M–N–C catalysts synthesized by this method using inexpensive precursors are promising choices for cathode catalysts for fuel cells.

Acknowledgements

The authors would like to acknowledge to DGIST R&D Program of the Ministry of Education, Science and Technology of Korea (15-BD-01) for financial support.

Notes and references

1 M. K. Debe, *Nature*, 2012, **486**, 43–51.
2 H. A. Gasteiger and N. M. Marković, *Science*, 2009, **324**, 48–49.
3 G. Cui, L. Zhi, A. Thomas, U. Kolb, I. Lieberwirth and K. Müllen, *Angew. Chem., Int. Ed.*, 2007, **46**, 3464–3467.
4 Y. Liu and W. E. Mustain, *J. Am. Chem. Soc.*, 2013, **135**, 530–533.
5 Z. Chen, D. Higgins, A. Yu, L. Zhang and J. Zhang, *Energy Environ. Sci.*, 2011, **4**, 3167–3192.
6 F. Jaouen, E. Proietti, M. Lefèvre, R. Chenitz, J.-P. Dodelet, G. Wu, H. T. Chung, C. M. Johnston and P. Zelenay, *Energy Environ. Sci.*, 2011, **4**, 114–130.
7 Z. Zhang, X. Wang, G. Cui, A. Zhang, X. Zhou, H. Xu and L. Gu, *Nanoscale*, 2014, **6**, 3540–3544.
8 R. Jasinski, *Nature*, 1964, **201**, 1212–1213.
9 Z. Yang, Z. Yao, G. Li, H. Nie, Z. Liu, X. Zhou, X. Chen and S. Huang, *ACS Nano*, 2012, **6**, 205–211.
10 R. Silva, D. Voiry, M. Chhowalla and T. Asefa, *J. Am. Chem. Soc.*, 2013, **135**, 7823–7826.
11 D.-W. Wang and D. Su, *Energy Environ. Sci.*, 2014, **7**, 576–591.
12 X. Zhao, J. Zhu, L. Liang, C. Li, C. Liu, J. Liao and W. Xing, *Appl. Catal., B*, 2014, **154**, 177–182.
13 H. Liang, X. Zhuang, S. Bru, X. Feng and K. Mu, *Nat. Commun.*, 2014, **5**, 4973.
14 H. T. Chung, J. H. Won and P. Zelenay, *Nat. Commun.*, 2013, **4**, 1922.
15 G. Wu, K. L. More, C. M. Johnston and P. Zelenay, *Science*, 2011, **332**, 443–447.
16 Y. Tan, C. Xu, G. Chen, X. Fang and N. Zheng, *Adv. Funct. Mater.*, 2012, **22**, 4584–4591.
17 E. Proietti, F. Jaouen, M. Lefèvre, N. Larouche, J. Tian, J. Herranz and J.-P. Dodelet, *Nat. Commun.*, 2011, **2**, 416.
18 J. Y. Cheon, T. Kim, Y. Choi, H. Y. Jeong, M. G. Kim, Y. J. Sa, J. Kim, Z. Lee, T. Yang, K. Kwon, O. Terasaki, G. Park, R. R. Adzic and S. H. Joo, *Sci. Rep.*, 2013, **3**, 2715–2723.
19 J. Sanetuntikul, T. Hang and S. Shanmugam, *Chem. Commun.*, 2014, **50**, 9473–9476.
20 H. Shi, J. N. Reimers and J. R. Dahn, *J. Appl. Crystallogr.*, 1993, **26**, 827–836.

21 H. Peng, Z. Mo, S. Liao, H. Liang, L. Yang, F. Luo, H. Song, Y. Zhong and B. Zhang, *Sci. Rep.*, 2013, **3**, 1765.
22 F. Tuinstra, *J. Chem. Phys.*, 1970, **53**, 1126–1130.
23 P. Marcus, *Corros. Sci.*, 1992, **33**, 805–814.
24 B. Jousselme, S. Palacin, A. Morozan and P. Je, *Phys. Chem. Chem. Phys.*, 2011, **13**, 21600–21607.
25 H. Huang, I. Shown, S. Chang, H. Hsu, H. Du, M. Kuo, K. Wong, S. Wang, C. Wang, L. Chen and K. Chen, *Adv. Funct. Mater.*, 2012, **22**, 3500–3508.
26 S. Shanmugam and T. Osaka, *Chem. Commun.*, 2011, **47**, 4463–4465.
27 N. K. Chaudhari, M. Y. Song and J. Yu, *Sci. Rep.*, 2014, **4**, 5221.
28 C. V. Rao, C. R. Cabrera and Y. Ishikawa, *J. Phys. Chem. Lett.*, 2010, **1**, 2622–2627.
29 A. Kong, X. Zhu, Z. Han, Y. Yu, Y. Zhang, B. Dong and Y. Shan, *ACS Catal.*, 2014, **4**, 1793–1800.
30 L. Feng, L. Yang, Z. Huang, J. Luo, M. Li, D. Wang and Y. Chen, *Sci. Rep.*, 2013, **3**, 3306.
31 N. Ramaswamy and S. Mukerjee, *Adv. Phys. Chem.*, 2012, **2012**, 1–17.
32 Y. Liang, *Nat. Mater.*, 2011, **10**, 780–786.
33 Y. Chang, F. Hong, C. He, Q. Zhang and J. Liu, *Adv. Mater.*, 2013, **25**, 4794–4799.
34 I. Kruusenberg, L. Matisen, Q. Shah, A. M. Kannan and K. Tammeveski, *Int. J. Hydrogen Energy*, 2012, **37**, 4406–4412.